Computational Methods for Differential Equations
http://cmde.tabrizu.ac.ir
Vol. 9, No. 2, 2021, pp. 358-374
DOI:10.22034/cmde.2019.30396.1450

Numerical investigation based on a local meshless radial point interpolation for solving coupled nonlinear reaction-diffusion system

Elyas Shivanian[*]
Department of Applied Mathematics,
Imam Khomeini International University, Qazvin, 34149-16818, Iran.
E-mail: shivanian@sci.ikiu.ac.ir

Ahmad Jafarabadi
Department of Applied Mathematics,
Imam Khomeini International University, Qazvin, 34149-16818, Iran.
E-mail: jafarabadi.ahmad@yahoo.com

Abstract In the present paper, the spectral meshless radial point interpolation (SMRPI) technique is applied to the solution of pattern formation in nonlinear reaction-diffusion systems. Firstly, we obtain a time discrete scheme by approximating the time derivative via a finite difference formula, then we use the SMRPI approach to approximate the spatial derivatives. This method is based on a combination of meshless methods and spectral collocation techniques. The point interpolation method with the help of radial basis functions is used to construct shape functions which act as basis functions in the frame of SMRPI. In the current work, the thin plate splines (TPS) are used as the basis functions and in order to eliminate the nonlinearity, a simple predictor-corrector (P-C) scheme is performed. The effect of parameters and conditions are studied by considering the well known Brusselator model. Two test problems are solved and numerical simulations are reported which confirm the efficiency of the proposed scheme.

Keywords. Turing systems; Brusselator model; Spectral meshless radial point interpolation (SMRPI) method; Radial basis function, Finite difference method.

2010 Mathematics Subject Classification. 65M99.

1. Introduction

As mentioned in [45], mathematical simulation of systems in developmental biology has given rise to a variety of models which account for spatial-temporal patterning phenomena. Many of these mathematical models are reaction-diffusion systems which have the general form

$$\frac{\partial u}{\partial t} = D\Delta u + F(u),$$

where $u \in \mathbb{R}^p$ represent concentrations of a group of biochemical molecules (p is the number of partial differential equations in the system and it can be $1, 2, 3$, etc.), $D \in \mathbb{R}^{p\times p}$ is the diffusion constant matrix, Δu is the Laplacian associated with the

Received: 15 November 2018 ; Accepted: 12 January 2020.

[*] corresponding author.

diffusion of the molecule whose concentration is u, and $F(u)$ describes the biochemical reactions. Examples include Turing-type models [43] such as the Gierer-Meinhardt model [11], Brusselator model [23], the Schnakenberg model [27], the Thomas model [42], the Gray-Scott model [12, 13] and others described in [3, 4, 6, 5, 25].

The present work considers the numerical solutions of the coupled pair of nonlinear partial differential equations in a general form as follows

$$\begin{cases} \dfrac{\partial u(\mathbf{x},t)}{\partial t} = D_1 \Delta u(\mathbf{x},t) + \alpha_1 u(\mathbf{x},t) + f_1(u,v) + g_1(\mathbf{x},t), \\[2ex] \dfrac{\partial v(\mathbf{x},t)}{\partial t} = D_2 \Delta v(\mathbf{x},t) + \alpha_2 v(\mathbf{x},t) + \alpha_3 u(\mathbf{x},t) + f_2(u,v) + g_2(\mathbf{x},t), \\[2ex] \mathbf{x} = (x,y) \in \Omega \subset \mathbb{R}^2, \qquad t \in [0,T], \end{cases} \tag{1.1}$$

with given initial and Dirichlet and/or Neumann's boundary conditions, where D_1, D_2, α_1, α_2 and α_3 are given constants, f_1 and f_2 are functions of the field variables u and v, g_1 and g_2 are assumed to be prescribed sources. Recall that in the case of two-component reaction system, $u(\mathbf{x},t)$ and $v(\mathbf{x},t)$ stand for concentrations and D_1, D_2 for the diffusion coefficients of chemical species [29]. Turing equations describe the temporal development of the morphogenic concentrations u and v which can be represented in general by the following coupled reaction-diffusion equations [21, 24]

$$\begin{cases} \dfrac{\partial u(\mathbf{x},t)}{\partial t} = \Delta u(\mathbf{x},t) + f(u,v), \\[2ex] \dfrac{\partial v(\mathbf{x},t)}{\partial t} = d \Delta v(\mathbf{x},t) + g(u,v), \end{cases} \tag{1.2}$$

where d represents the relative magnitude of the diffusion coefficient of one morphogen compared to the other and f and g are reaction kinetics. A spatially-uniform steady state of the above system is the state (u_s, v_s) for which $f(u_s, v_s) = 0$ and $g(u_s, v_s) = 0$. If system (1.2) is considered, the boundary conditions are usually taken as the Neumann type

$$\frac{\partial u}{\partial \mathbf{n}} = 0, \qquad \frac{\partial v}{\partial \mathbf{n}} = 0, \qquad \text{on } \partial\Omega, \tag{1.3}$$

where $\mathbf{n}$ denotes the unit outward normal vector on $\partial\Omega$, the boundary of region Ω.

The reaction-diffusion system is used to describe the Turing models. Turing systems appear in various biological systems, such as patterns in fish, butterflies and ladybugs [15, 17]. A brief and historical review on numerical methods for solving turing systems is given in Ref. [8] that some examples are described below. In [44], a second-order scheme has been proposed for the Brusselator reaction-diffusion system. The authors of [19] examined the implications of mesh structure on numerically computed solutions of a well-studied reaction-diffusion system on two-dimensional fixed and growing domains. Zhu et al. [45] applied discontinuous Galerkin (DG) finite element methods, coupled with Strang type symmetrical operator splitting methods for solving reaction-diffusion systems in domains with complex geometry. Shakeri and Dehghan [28] combined the spectral element method and finite volume technique for numerical solution of the reaction-diffusion Schnakenberg model of Turing type. Shirzadi et al. [29] used weak formulations of general reaction-diffusion problems on local subdomains with using a meshless approximation for field variables. Madzvamuse and Chung [18] proposed fully implicit time-stepping schemes and nonlinear solvers for systems of reaction-diffusion equations. The main contribution of their paper is the study of fully implicit schemes by use of the Newton method and the Picard iteration applied to the backward Euler, the Crank-Nicolson (and its modifications) and the fractional-step θ methods. The authors of [41] proposed a meshless local integral equation (LIE) method for numerical simulation of $2D$ pattern formation in nonlinear reaction diffusion systems. Dehghan et al. [8] solved some Turing models using a meshless method that is called element free Galerkin (EFG) approach based on moving Kriging and radial point interpolation shape functions. They obtained the numerical simulations of some Turing models such as Schnakenberg model, Gierer-Meinhardt model, Morphodynamic model, FitzHugh-Nagumo monodomain model-I and FitzHugh-Nagumo monodomain model-II.

The main aim of the current paper is to develop a combined local meshless radial point interpolation approach so-called spectral meshless radial point interpolation (SMRPI) method to solve coupled nonlinear reaction-diffusion system (1.1). This method is based on meshless radial point interpolation and spectral collocation techniques which have already been used in some articles such as [16, 36, 38, 39]. Also, see [2, 7, 9, 10, 14, 20, 22, 26, 30, 31, 32, 34, 35, 40] for more information about meshfree methods.

The structure of this article is as follows: we will discretize the temporal dimension using a finite difference scheme in section 2. The implementation of the SMRPI for time discrete equation is given in section 3. In section 4, we report the numerical experiments of solving the considered models for two test problems. Finally, a brief conclusion of the current paper has been written in section 5.

2. Time discrete scheme

Let us define

$$t_k = k\delta t, \qquad k = 0, 1, ..., M,$$

where $\delta t = T/M$ is the step size of time variable. In this section, we discretize the time variable using forward finite difference relation for the first order derivatives on time variable with the Crank-Nicolson scheme, appropriately, as follows

$$\frac{\partial u(\mathbf{x},t)}{\partial t} \cong \frac{u^{k+1}(\mathbf{x}) - u^k(\mathbf{x})}{\delta t}, \tag{2.1}$$

$$\Delta u(\mathbf{x},t) \cong \frac{1}{2}\big(\Delta u^{k+1}(\mathbf{x}) + \Delta u^k(\mathbf{x})\big), \tag{2.2}$$

where $u^{k+1}(\mathbf{x})$ is approximate solution at the point $(\mathbf{x}, t_{k+1})$. Applying the above approximation and impose them to the original Eq. (1.1), we are conducted to the following time discrete equation:

$$\left\{\begin{aligned}
\frac{u^{k+1}(\mathbf{x})-u^{k}(\mathbf{x})}{\delta t} &= \frac{D_1}{2}\big(\Delta u^{k+1}(\mathbf{x})+\Delta u^{k}(\mathbf{x})\big)+\frac{\alpha_1}{2}\big(u^{k+1}(\mathbf{x})+u^{k}(\mathbf{x})\big)\\
&\quad +f_1(u^k,v^k)+\frac{1}{2}\big(g_1^{k+1}(\mathbf{x})+g_1^{k}(\mathbf{x})\big),\\
\frac{v^{k+1}(\mathbf{x})-v^{k}(\mathbf{x})}{\delta t} &= \frac{D_2}{2}\big(\Delta v^{k+1}(\mathbf{x})+\Delta v^{k}(\mathbf{x})\big)+\frac{\alpha_2}{2}\big(v^{k+1}(\mathbf{x})+v^{k}(\mathbf{x})\big)\\
&\quad +\frac{\alpha_3}{2}\big(u^{k+1}(\mathbf{x})+u^{k}(\mathbf{x})\big)+f_2(u^k,v^k)+\frac{1}{2}\big(g_2^{k+1}(\mathbf{x})+g_2^{k}(\mathbf{x})\big),
\end{aligned}\right. \tag{2.3}$$

Then, Eq. (2.3) can be rewritten as

$$\left\{\begin{aligned}
&(\lambda-\alpha_1)u^{k+1}(\mathbf{x})-D_1\Delta u^{k+1}(\mathbf{x}) = (\lambda+\alpha_1)u^{k}(\mathbf{x})+D_1\Delta u^{k}(\mathbf{x})\\
&\qquad\qquad +2f_1(u^k,v^k)+G_1^{k+1}(\mathbf{x}),\\
&(\lambda-\alpha_2)v^{k+1}(\mathbf{x})-D_2\Delta v^{k+1}(\mathbf{x})-\alpha_3 u^{k+1}(\mathbf{x}) = (\lambda+\alpha_2)v^{k}(\mathbf{x})+D_2\Delta v^{k}(\mathbf{x})\\
&\qquad\qquad +\alpha_3 u^k+2f_2(u^k,v^k)+G_2^{k+1}(\mathbf{x}),
\end{aligned}\right. \tag{2.4}$$

where $\lambda = 2/\delta t$, $G_i^{k+1}(\mathbf{x}) = g_i^{k+1}(\mathbf{x})+g_i^{k}(\mathbf{x})$, $i=1,2$.

3. Numerical implementation for the SMRPI method

Based on the proposed method in [33], the contents of this section are coming up. Firstly, we introduce some notations of derivatives and then we apply the SMRPI to system (2.4). In the current work, we assume that the number of total nodes covering $\overline{\Omega} = (\Omega\cup\partial\Omega)$ is N. Also, we consider that the $n_{\mathbf{x}}$ is the number of nodes included in support domain $\Omega_{\mathbf{x}}$ corresponding to the point of interest $\mathbf{x}=(x,y)$. For example $\Omega_{\mathbf{x}}$ can be a disk centered at $\mathbf{x}$ with radius r_s. By the idea of interpolation, a continuous function $u(\mathbf{x})$ at a point of interest $\mathbf{x}$ is approximated in the form of

$$u(\mathbf{x}) = \mathbf{\Phi}^{tr}(\mathbf{x})\mathbf{U}_s = \sum_{j=1}^{N}\phi_j(\mathbf{x})u_j. \tag{3.1}$$

Since corresponding to node $\mathbf{x}_j$ there is a shape function $\phi_j(\mathbf{x}), j=1,2,...,N$, we define $\Omega_{\mathbf{x}}^c = \{\mathbf{x}_j : \mathbf{x}_j \notin \Omega_{\mathbf{x}}\}$. Thus to guarantee the Kronecker delta function property, we set

$$\forall\mathbf{x}_j\in\Omega_{\mathbf{x}}^c : \phi_j(\mathbf{x}) = 0. \tag{3.2}$$

Now the derivatives of $u(\mathbf{x})$ with respect to x and y are

$$\frac{\partial u(\mathbf{x})}{\partial x} = \sum_{j=1}^{N} \frac{\partial \phi_j(\mathbf{x})}{\partial x} u_j, \qquad \frac{\partial u(\mathbf{x})}{\partial y} = \sum_{j=1}^{N} \frac{\partial \phi_j(\mathbf{x})}{\partial y} u_j, \tag{3.3}$$

and for higher order derivatives of $u(\mathbf{x})$, we have

$$\frac{\partial^s u(\mathbf{x})}{\partial x^s} = \sum_{j=1}^{N} \frac{\partial^s \phi_j(\mathbf{x})}{\partial x^s} u_j, \qquad \frac{\partial^s u(\mathbf{x})}{\partial y^s} = \sum_{j=1}^{N} \frac{\partial^s \phi_j(\mathbf{x})}{\partial y^s} u_j, \tag{3.4}$$

where $\dfrac{\partial^s(.)}{\partial x^s}$ and $\dfrac{\partial^s(.)}{\partial y^s}$ are s'th derivatives with respect to x and y. Now, by substituting $\mathbf{x} = (x_i, y_i)$ into above equations

$$U_x^{(s)} = D_x^{(s)} U, \qquad U_y^{(s)} = D_y^{(s)} U, \tag{3.5}$$

where

$$U_x^{(s)} = \left(u_{x_1}^{(s)}, u_{x_2}^{(s)}, ..., u_{x_N}^{(s)}\right)^{tr}, \qquad U_y^{(s)} = \left(u_{y_1}^{(s)}, u_{y_2}^{(s)}, ..., u_{y_N}^{(s)}\right)^{tr}, \tag{3.6}$$

$$D_{x_{ij}}^{(s)} = \frac{\partial^s \phi_j(\mathbf{x}_i)}{\partial x^s}, \qquad D_{y_{ij}}^{(s)} = \frac{\partial^s \phi_j(\mathbf{x}_i)}{\partial y^s}, \tag{3.7}$$

and

$$U = (u_1, u_2, ..., u_N)^{tr}. \tag{3.8}$$

It is necessary that we mention $\forall \mathbf{x}_j \in \Omega_{\mathbf{x}}^c : \partial^s \phi_j(\mathbf{x})/\partial x^s = \partial^s \phi_j(\mathbf{x})/\partial y^s = 0, s = 1, 2, \ldots$, due to Eq. (3.2).

In the second step of this section, we implement the SMRPI method to the discrete system (2.4) with initial conditions

$$u(\mathbf{x}, 0) = u_0(\mathbf{x}), \qquad v(\mathbf{x}, 0) = v_0(\mathbf{x}), \qquad \mathbf{x} \in \Omega, \tag{3.9}$$

and Dirichlet boundary conditions

$$u(\mathbf{x}, t) = h_1(\mathbf{x}, t), \qquad v(\mathbf{x}, t) = h_2(\mathbf{x}, t), \qquad \mathbf{x} \in \partial\Omega, \qquad t > 0. \tag{3.10}$$

To impose Neumann's boundary conditions, i.e. Eq. (1.3), we adopt our proposed method in [37]. We consider N nodes with arbitrary distribution on the boundary and domain of the problem. Assuming that $\{u(\mathbf{x}_i, k\delta t), v(\mathbf{x}_i, k\delta t)\}_{i=1}^{N}$ are known, and our aim is to compute $\{u(\mathbf{x}_i, (k+1)\delta t), v(\mathbf{x}_i, (k+1)\delta t)\}_{i=1}^{N}$. So, we have $2N$ unknown values and to compute these unknown values, we need $2N$ equations. As was described, corresponding to each node we obtain one equation. Now, by substituting of the points $\mathbf{x}_i$, $i = 1, 2, ..., N_\Omega$,(the interior points of Ω), into the system (2.4), and using approximate formulas (3.1)-(3.4), Eq. (2.4) is written as follows:

$$\begin{cases}
(\lambda-\alpha_1)\sum_{j=1}^{N}\phi_j(x_i,y_i)u_j^{k+1}-D_1\big(\sum_{j=1}^{N}\dfrac{\partial^2\phi_j(x_i,y_i)}{\partial x^2}u_j^{k+1}+\sum_{j=1}^{N}\dfrac{\partial^2\phi_j(x_i,y_i)}{\partial y^2}u_j^{k+1}\big)\\
=(\lambda+\alpha_1)\sum_{j=1}^{N}\phi_j(x_i,y_i)u_j^{k}+D_1\big(\sum_{j=1}^{N}\dfrac{\partial^2\phi_j(x_i,y_i)}{\partial x^2}u_j^{k}+\sum_{j=1}^{N}\dfrac{\partial^2\phi_j(x_i,y_i)}{\partial y^2}u_j^{k}\big)\\
+2\Psi_1^k(x_i,y_i)+G_1^{k+1}(x_i,y_i),\\
(\lambda-\alpha_2)\sum_{j=1}^{N}\phi_j(x_i,y_i)v_j^{k+1}-D_2\big(\sum_{j=1}^{N}\dfrac{\partial^2\phi_j(x_i,y_i)}{\partial x^2}v_j^{k+1}+\sum_{j=1}^{N}\dfrac{\partial^2\phi_j(x_i,y_i)}{\partial y^2}v_j^{k+1}\big)\\
-\alpha_3\sum_{j=1}^{N}\phi_j(x_i,y_i)u_j^{k+1}=(\lambda+\alpha_2)\sum_{j=1}^{N}\phi_j(x_i,y_i)v_j^{k}+\alpha_3\sum_{j=1}^{N}\phi_j(x_i,y_i)u_j^{k}\\
+D_2\big(\sum_{j=1}^{N}\dfrac{\partial^2\phi_j(x_i,y_i)}{\partial x^2}v_j^{k}+\sum_{j=1}^{N}\dfrac{\partial^2\phi_j(x_i,y_i)}{\partial y^2}v_j^{k}\big)+2\Psi_2^k(x_i,y_i)+G_2^{k+1}(x_i,y_i),
\end{cases}\tag{3.11}$$

for $i=1,2,...,N_\Omega$, where $\Psi_l^k(x_i,y_i)=f_l\big(u^k(x_i,y_i),v^k(x_i,y_i)\big)$, $l=1,2$. From Eq. (3.2) and the notations (3.7), we can conclude

$$\begin{cases}
(\lambda-\alpha_1)u_i^{k+1}-D_1\sum_{j=1}^{N}\big(D_{x_{ij}}^{(2)}+D_{y_{ij}}^{(2)}\big)u_j^{k+1}=(\lambda+\alpha_1)u_i^k+D_1\sum_{j=1}^{N}\big(D_{x_{ij}}^{(2)}+D_{y_{ij}}^{(2)}\big)u_j^k\\
\qquad\qquad\qquad\qquad\qquad\qquad\qquad+2\Psi_1^k(x_i,y_i)+G_1^{k+1}(x_i,y_i),\\
(\lambda-\alpha_2)v_i^{k+1}-D_2\sum_{j=1}^{N}\big(D_{x_{ij}}^{(2)}+D_{y_{ij}}^{(2)}\big)v_j^{k+1}-\alpha_3u_i^{k+1}\\
\quad=(\lambda+\alpha_2)v_i^k+D_2\sum_{j=1}^{N}\big(D_{x_{ij}}^{(2)}+D_{y_{ij}}^{(2)}\big)v_j^k+\alpha_3u_i^k+2\Psi_2^k(x_i,y_i)+G_2^{k+1}(x_i,y_i),
\end{cases}\tag{3.12}$$

where $i=1,2,...,N_\Omega$. For nodes which are located on the boundary of Ω, i.e. $\partial\Omega$, using Eq. (3.10), we have the following relations

$$u_i^{k+1}=h_1^{k+1}(x_i,y_i),\qquad v_i^{k+1}=h_2^{k+1}(x_i,y_i),\qquad i=1,2,...,N_{\partial\Omega}.\tag{3.13}$$

Suppose that N is the total number of nodes covering $\bar{\Omega}$, i.e. $N=N_\Omega+N_{\partial\Omega}$. If we show the sparse system as the following matrix form

$$\mathbf{A}\mathbf{U}^{k+1}=\mathbf{B}\mathbf{U}^k+\mathbf{F}^{k+1}+\mathbf{C},\tag{3.14}$$

then, above matrices are defined as follows:

$$\mathbf{A}=\begin{pmatrix}[A_1]_{N\times N} & [0]_{N\times N}\\ [A_2]_{N\times N} & [A_3]_{N\times N}\end{pmatrix}_{2N\times 2N},\tag{3.15}$$

where A_1, A_2 and A_3 are for $j=1,2,...,N$, as follows

$$(A_1)_{ij}=\begin{cases}(\lambda-\alpha_1)\delta_{ij}-D_1\big(D_{x_{ij}}^{(2)}+D_{y_{ij}}^{(2)}\big) & ,i=1,2,...,N_\Omega\\ \delta_{ij} & ,i=N_\Omega+1,...,N\end{cases}\tag{3.16}$$

$$(A_2)_{ij} = \begin{cases} -\alpha_3\delta_{ij} & , i = 1, 2, ..., N_\Omega \\ 0 & , i = N_\Omega + 1, ..., N \end{cases} \tag{3.17}$$

$$(A_3)_{ij} = \begin{cases} (\lambda - \alpha_2)\delta_{ij} - D_2\big(D^{(2)}_{x_{ij}} + D^{(2)}_{y_{ij}}\big) & , i = 1, 2, ..., N_\Omega \\ \delta_{ij} & , i = N_\Omega + 1, ..., N \end{cases} \tag{3.18}$$

$$\mathbf{B} = \begin{pmatrix} [B_1]_{N\times N} & [0]_{N\times N} \\ [B_2]_{N\times N} & [B_3]_{N\times N} \end{pmatrix}_{2N\times 2N}, \tag{3.19}$$

where B_1, B_2 and B_3 are as follows

$$(B_1)_{ij} = \begin{cases} (\lambda + \alpha_1)\delta_{ij} + D_1\big(D^{(2)}_{x_{ij}} + D^{(2)}_{y_{ij}}\big) & , i = 1, 2, ..., N_\Omega \\ 0 & , i = N_\Omega + 1, ..., N \end{cases} \tag{3.20}$$

$$(B_2)_{ij} = \begin{cases} \alpha_3\delta_{ij} & , i = 1, 2, ..., N_\Omega \\ 0 & , i = N_\Omega + 1, ..., N \end{cases} \tag{3.21}$$

$$(B_3)_{ij} = \begin{cases} (\lambda + \alpha_2)\delta_{ij} + D_2\big(D^{(2)}_{x_{ij}} + D^{(2)}_{y_{ij}}\big) & , i = 1, 2, ..., N_\Omega \\ 0 & , i = N_\Omega + 1, ..., N \end{cases} \tag{3.22}$$

$$\mathbf{F}^{k+1} = \begin{pmatrix} [F_1]_{N\times 1} \\ [F_2]_{N\times 1} \end{pmatrix}_{2N\times 1}, \qquad \mathbf{C} = \begin{pmatrix} [C_1]_{N\times 1} \\ [C_2]_{N\times 1} \end{pmatrix}_{2N\times 1}, \tag{3.23}$$

where new matrixes are as follows

$$(F_1)_i = G_1^{k+1}(x_i, y_i), \quad (F_2)_i = G_2^{k+1}(x_i, y_i), \quad \text{for} \quad i = 1, 2, ..., N_\Omega, \tag{3.24}$$

$$(F_1)_i = h_1^{k+1}(x_i, y_i), \quad (F_2)_i = h_2^{k+1}(x_i, y_i), \quad \text{for} \quad i = N_\Omega + 1, 2, ..., N, \tag{3.25}$$

$$(C_1)_i = 2\Psi_1^k(x_i, y_i), \quad (C_2)_i = 2\Psi_2^k(x_i, y_i), \quad \text{for} \quad i = 1, 2, ..., N_\Omega, \tag{3.26}$$

$$(C_1)_i = 0, \quad (C_2)_i = 0, \quad \text{for} \quad i = N_\Omega + 1, 2, ..., N, \tag{3.27}$$

and finally, the vector of unknown values is

$$\mathbf{U}^{k+1} = \Big(u_1^{k+1}, u_2^{k+1}, ..., u_N^{k+1}, v_1^{k+1}, v_2^{k+1}, ..., v_N^{k+1}\Big)^{tr}. \tag{3.28}$$

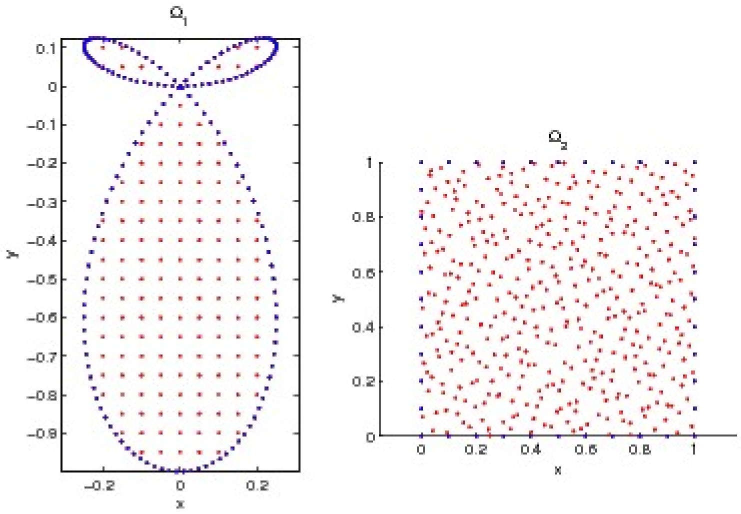

FIGURE 1. Considered domains in the current paper.

At the first time level, when $k = 0$, according to Eq. (3.9), we apply the following assumption:

$$\mathbf{U}^0 = \begin{pmatrix} [\mathbf{u}_0]_{N\times 1} \\ \\ [\mathbf{v}_0]_{N\times 1} \end{pmatrix}_{2N\times 1}, \tag{3.29}$$

where

$$\mathbf{u}_0 = \Big(u_0(x_1, y_1), u_0(x_2, y_2), ..., u_0(x_N, y_N) \Big)^{tr},$$

$$\mathbf{v}_0 = \Big(v_0(x_1, y_1), v_0(x_2, y_2), ..., v_0(x_N, y_N) \Big)^{tr}.$$

In the above Equations, δ_{ij} is the Kronecker delta function, i.e.

$$\delta_{ij} = \begin{cases} 1 & , i = j \\ 0 & , i \neq j \end{cases}. \tag{3.30}$$

To keep away from solving a nonlinear algebraic system of equations and obtaining the acceptable numerical results, the authors of [8] used a predictor-corrector algorithm. We likewise use same procedure for dealing with the nonlinearity as Eq. (3.26).

4. Numerical results

In this section, we present the numerical results of the proposed method on two test problems. In the first example, we use the maximum absolute error as the error criterion. In the second example, due to unavailability of exact solutions, we consider two strategies for examining the obtained numerical results as follows [8]:

(1) For checking the stability of time difference scheme, we use the following strategy:

$$E^n_{\delta t} = \frac{\| \mathbf{U}^n - \mathbf{U}^{n-1} \|_\infty}{\| \mathbf{U}^n \|_\infty} \tag{4.1}$$

in which $\mathbf{U}^n$ is the numerical solution at (n)'th iteration.

(2) For checking the convergence of full discrete scheme, we use the following strategy. We consider the obtained solution with $h_{RS} = 1/32$ (in the current work) as a reference solution (as an exact solution) and then we run our MATLAB program for different values of h that results the numerical solution S^N_h (numerical solution using the method presented in the current paper). Now, interpolating the reference solution at the points with spatial step size h, we obtain the numerical solution S^I_h $\big($numerical solution using MATLAB command "interp2(.,'spline')"$\big)$. Finally, we define the following error relation:

$$E_h = \| S^N_h - S^I_h \|_\infty . \tag{4.2}$$

In the current work, we have chosen TPS as radial basis function as follows:

$$R(\mathbf{x}) = r^{2\lambda} \ln(r), \qquad r = \sqrt{\mathbf{x} - \mathbf{x}_i}, \qquad \lambda = 1, 2, ..., \tag{4.3}$$

corresponding to the support domain at central point $\mathbf{x}_i$. For the second-order partial differential equation (1.1), $\lambda = 2$ is used for thin plate splines and also in test problems, we set $r_s = 4.2h$ as the radius of support domain. Fig. 1 presents the considered irregular domains in test problems which are defined as follows: the circumference of Ω_1 is $r = \sin\theta \cos 2\theta$, where $0 \leq \theta \leq 2\pi$, and Ω_2 presents the irregular distribution of collocation nodes covering the domain $[0, 1]^2$ (using the MATLAB routine 'haltonset').

Example 4.1. Consider the following system

$$\begin{cases} \dfrac{\partial u}{\partial t} = \Delta u + u - u^2 v^2 + g_1(x, y, t), \\ \\ \dfrac{\partial v}{\partial t} = \Delta v + v - u^2 + uv + g_2(x, y, t). \end{cases} \tag{4.4}$$

Initial and Dirichlet boundary conditions with prescribed sources g_1, g_2 can be obtained from the following exact solutions which is given by Ref. [29]

$$u(x, y, t) = exp(-2t + x + y), \qquad v(x, y, t) = exp(-t + x - y). \tag{4.5}$$

Table 1 presents the absolute errors on $[0, 1]^2$ with $h = 1/10$ at $T = \{1, 5\}$ for some different step sizes δt. Fig. 2 demonstrates the graphs of approximate solution and absolute error for $u(x, y, t)$ and $v(x, y, t)$ with $h = 1/20$, $\delta t = 0.01$ at $T = 1$ on Ω_1. Clearly, the present method is accurate for the irregular domain Ω_1. Fig. 3 displays the graphs of absolute error for $u(x, y, t)$ and $v(x, y, t)$ with $N = 256$, $\delta t = 0.01$ at different time levels up to $T = 4$ on Ω_2. From Fig. 3, it is understood that the accuracy of the method does not depend on the type of distribution points.

TABLE 1. Numerical results of absolute errors on $[0,1]^2$ with $h = 1/10$ for Example 4.1.

	$T = 1$		$T = 5$	
δt	$L_\infty(u)$	$L_\infty(v)$	$L_\infty(u)$	$L_\infty(v)$
$\delta t = 1/10$	$2.2747e-04$	$2.1832e-05$	$4.3904e-07$	$4.9764e-07$
$\delta t = 1/20$	$5.5953e-05$	$5.3558e-06$	$1.9217e-08$	$1.2246e-07$
$\delta t = 1/40$	$1.3931e-05$	$1.2767e-06$	$4.7854e-09$	$2.9496e-08$
$\delta t = 1/80$	$3.4204e-06$	$2.7807e-07$	$1.1747e-09$	$6.2459e-09$

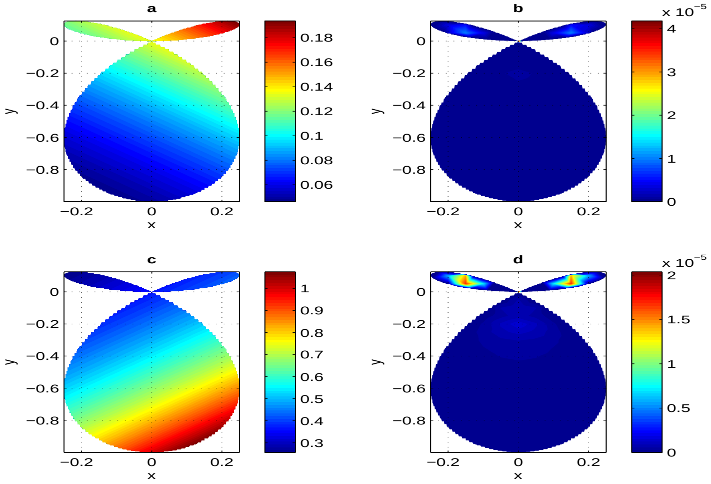

FIGURE 2. Graphs of approximate solution (left panel) and absolute error (right panel) for $u(x, y, t)$ (a, b) and $v(x, y, t)$ (c, d), respectively, with $h = 1/20$, $\delta t = 0.01$ at $T = 1$ on Ω_1 for Example 4.1.

Example 4.2. The partial differential equations associated with the "Brusselator" system are given by (see, for instance, [1])

$$\begin{cases} \dfrac{\partial u}{\partial t} = \alpha \Delta u - (A+1)u + u^2 v + B, \\ \dfrac{\partial v}{\partial t} = \alpha \Delta v + Au - u^2 v, \end{cases} \tag{4.6}$$

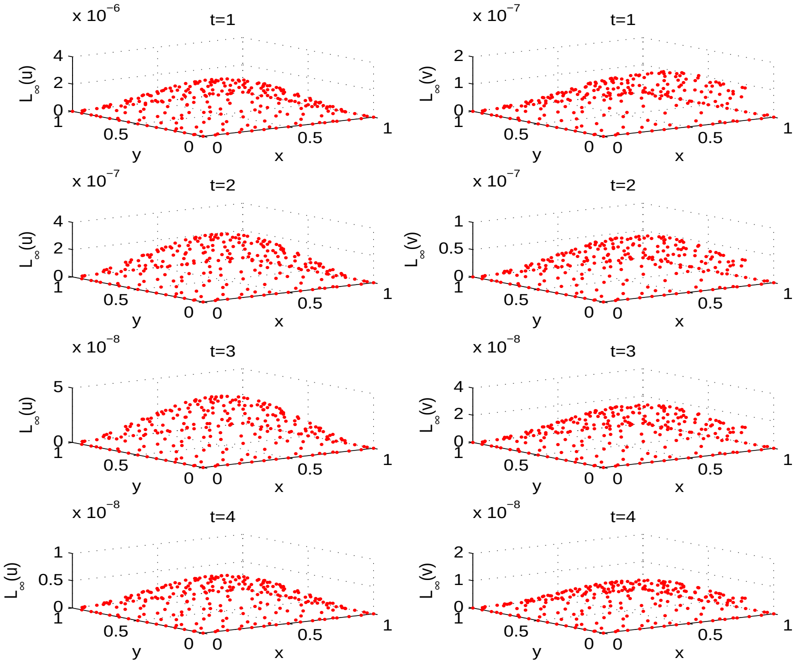

FIGURE 3. Graphs of absolute errors for $u(x,y,t)$ (left panel) and $v(x,y,t)$ (right panel) with $N = 256$, $\delta t = 0.01$ at different time levels up to $T = 4$ on Ω_2 for Example 4.1.

subject to the boundary conditions as Eq. (1.3). In this model, we assume that $\alpha = 0.002$, $A = 1$ and $B = 2$ with initial conditions as follows (Ref. [44])

$$u(x,y,0) = 2 + 0.25y, \qquad v(x,y,0) = 1 + 0.8x, \qquad (x,y) \in [0,1]^2. \quad (4.7)$$

When $(A,B) \neq (1,2)$, we use the following initial conditions (Ref. [29])

$$u(x,y,0) = \frac{1}{2}x^2 - \frac{1}{3}x^3, \qquad v(x,y,0) = \frac{1}{2}y^2 - \frac{1}{3}y^3, \qquad (x,y) \in [0,1]^2. \quad (4.8)$$

Tables 2 and 3 show the obtained errors corresponding to $E^n_{\delta t}$ and E_h, by present method. In these tables, we consider the numerical results with $h = 1/20$, $\delta t = 0.001$, $T = 1$ (for Table 2), $\delta t = 0.001$ and $T = 1$ (for Table 3).

In Tables 2 and 3, we put different value of A, B, namely $(A,B) \in \{(1/2,1),(1/2,1/2),(3/4,1/3),(1/2,1/5),(2/3,2/3)\}$ (by assumption (4.8)) and $(A,B) = (1,2)$ (by assumption (4.7)) . Stability, convergence and acceptable accuracy of SMRPI are visible from Tables 2 and 3. Moreover, as we see CPU time and condition number are acceptable. It is well known whenever the parameters A and B are chosen such that

TABLE 2. The obtained errors corresponding to $E^n_{\delta t}$ with $h = 1/20$, $\delta t = 0.001$ and $T = 1$ on $[0,1]^2$ for Example 4.2.

	Iterations	$A=1/2, B=1$	$A=1/2, B=1/2$	$A=1, B=2$
$u(x,y,t)$	200	$2.5089e-03$	$1.7695e-03$	$8.4542e-04$
	400	$1.4195e-03$	$1.1407e-03$	$2.7705e-04$
	600	$9.1353e-04$	$7.7636e-04$	$3.6074e-04$
	800	$6.3627e-04$	$5.4813e-04$	$3.3176e-04$
	1000	$4.7029e-04$	$3.9805e-04$	$2.8905e-04$
$v(x,y,t)$	200	$7.8577e-04$	$5.7423e-04$	$4.7095e-03$
	400	$8.6944e-04$	$5.8706e-04$	$1.4238e-03$
	600	$8.4682e-04$	$5.7173e-04$	$3.1484e-04$
	800	$7.7759e-04$	$5.4252e-04$	$2.3463e-04$
	1000	$6.9362e-04$	$5.0772e-04$	$2.3917e-04$
	Cond(A)	$9.3808e+02$	$9.3808e+02$	$9.3796e+02$
	CPU time(s)	46.154669	46.618334	47.000256

$1 - A + B^2 > 0$, the concentration profiles of u and v converge to the fixed point $(u, v) = (B, A/B)$, and for values of A and B such that $1-A+B^2 < 0$, the numerical method is seen not to converge to any fixed concentration (see Ref. [44]). To verify the convergence properties of the numerical scheme, we depict this fact in Figs. (4)-(7). We have shown the graphs of approximate solution for $u(x, y, t)$ and $v(x, y, t)$ with $A = 1/2, B = 1$, $h = 1/24$, $\delta t = 0.01$ at time levels up to $T = 10$ on $[0, 1]^2$ in Fig. 4. It is seen that Fig. 4 shows similar trends as the ones obtained by the method of local integral equation in Ref. [29]. Graphs of approximate solution for $u(x, y, t)$ and $v(x, y, t)$ versus the time with $h = 1/24$, $\delta t = 0.01$, $A = 1/2$, $B = 1$ at several mesh points, have been shown in Fig. (5). We present the graphs of approximate solution for $u(x, y, t)$ and $v(x, y, t)$ versus the time with $h = 1/10$, $\delta t = 0.01$, $A = 1$, $B = 2$ at several mesh points, in Fig. (6). It is clear from Figs. (4)-(6) that, for these values of h, δt and α, the numerical method is stable for this combination of A and B. Fig. (7) depicts profiles for u and v with $h = 1/10$, $\delta t = 0.01$, $A = 3$, $B = 1$ at several mesh points. It is apprehensible from Fig. (7) that the solution is unstable.

5. Conclusion

In this article, the SMRPI has been applied to the numerical solution of nonlinear reaction diffusion systems. For discretization, firstly, we discretized the time derivative using a finite difference formula and obtained a time discrete scheme. For the spatial variable, we used the shape functions which are constructed locally by the help

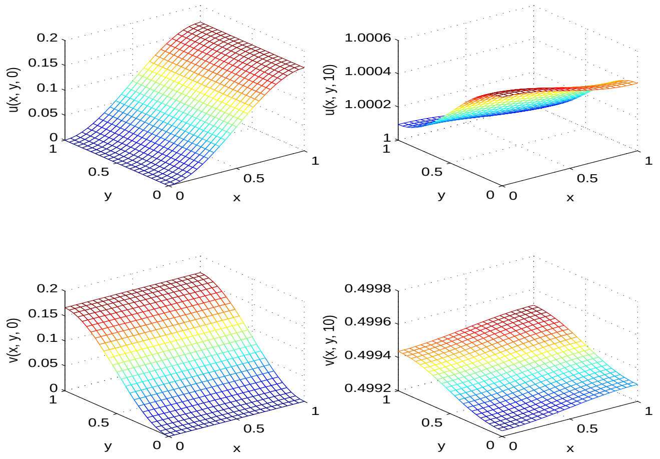

FIGURE 4. Graphs of approximate solution for $u(x, y, t)$ and $v(x, y, t)$ with $h = 1/24$, $\delta t = 0.01$, $A = 1/2$, $B = 1$ at $T = 0$ (left panel) and $T = 10$ (right panel) on $[0, 1]^2$ for Example 4.2.

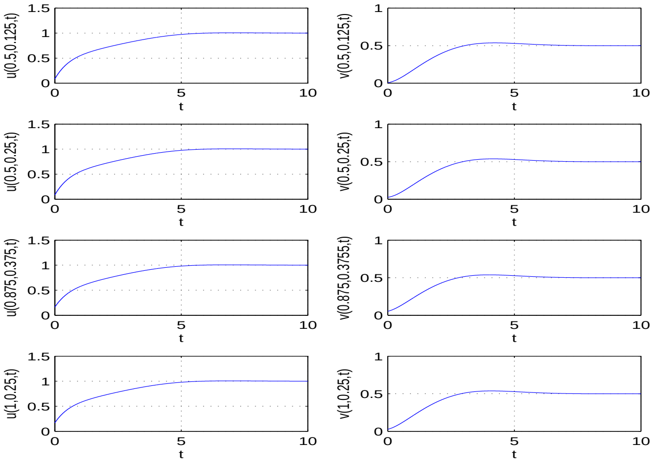

FIGURE 5. Graphs of approximate solution for $u(x, y, t)$ and $v(x, y, t)$ versus the time with $h = 1/24$, $\delta t = 0.01$, $A = 1/2$, $B = 1$ at some different mesh points for Example 4.2.

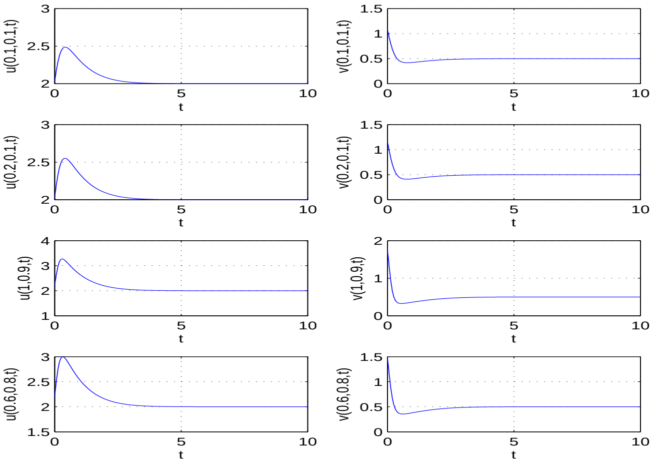

FIGURE 6. Graphs of approximate solution for $u(x, y, t)$ and $v(x, y, t)$ versus the time with $h = 1/10$, $\delta t = 0.01$, $A = 1$, $B = 2$ at some different mesh points for Example 4.2.

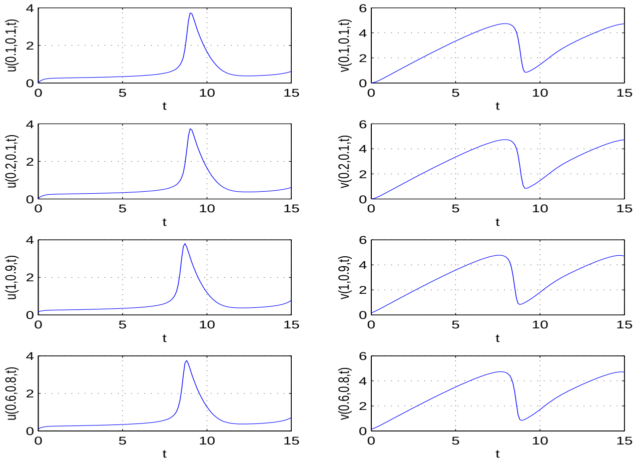

FIGURE 7. Graphs of approximate solution for $u(x, y, t)$ and $v(x, y, t)$ versus the time with $h = 1/10$, $\delta t = 0.01$, $A = 3$, $B = 1$ at some different mesh points for Example 4.2.

Table 3. The obtained errors corresponding to E_h with $\delta t = 0.001$ and $T = 1$ on $[0,1]^2$ for Example 4.2.

	h	$A = 3/4, B = 1/3$	$A = 1/2, B = 1/5$	$A = B = 2/3$
$u(x,y,t)$	$1/10$	$1.6964e-05$	$2.0113e-05$	$2.3081e-05$
	$1/20$	$3.1883e-06$	$3.9478e-06$	$4.2095e-06$
	$1/26$	$1.0619e-06$	$1.3182e-06$	$1.2929e-06$
$v(x,y,t)$	$1/10$	$1.0077e-04$	$9.4067e-05$	$9.5708e-05$
	$1/20$	$2.0851e-05$	$1.9552e-05$	$1.9711e-05$
	$1/26$	$6.4676e-06$	$6.0565e-06$	$6.1082e-06$

of the combination of thin plate radial basis functions and complete set of monomials via interpolation technique. The applicability of the developed formulation to simulations of patterns formation in reaction-diffusion systems has been verified on the well known Brusselator model. Because the conditions under which patterns formation is expected are known from the linear stability analysis, we could easily verify the ability of the developed formulation to result in the formation of patterns if the parameters of the model fall into the Turing space. Numerical experiments show the accord of the approximate solutions with those presented in [29, 44].

Acknowledgments

The authors are grateful to the reviewers for carefully reading this paper and for their comments and suggestions which have improved the paper.

Competing interests The authors declare that they have no competing interests.

Authors contributions All authors contributed equally to the writing of this paper. All authors read and approved the final manuscript.

References

[1] G. Adomian, *The diffusion-brusselator equation. Computers & Mathematics with Applications*, *29*(5) (1995), 13.

[2] F. A. Ghassabzade, J. SaberiNadjafi, and A. R. Soheili, *A method based on the meshless approach for singularly perturbed differential-difference equations with boundary layers*, Computational Methods for Differential Equations, *6*(3) (2018), 295311.

[3] J. L. Aragón, M. Torres, D. Gil, R. A. Barrio, and P. K. Maini, *Turing patterns with pentagonal symmetry,* Physical Review E, *65*(5) (2002), 051913.

[4] J. L. Aragón, C. Varea, R.A. Barrio, and P.K. Maini, *Spatial patterning in modified turing systems: Application to pigmentation patterns on marine fish*, Forma, *13*(3) (1998), 213221.

[5] R. A. Barrio, P. K. Maini, J. L. Aragón, and M. Torres, *Size-dependent symmetry breaking in models for morphogenesis*, Physica D: Nonlinear Phenomena, *168* (2002), 6172.

[6] R. A. Barrio, C. Varea, J. L. Aragón, and P. K. Maini, *A two-dimensional numerical study of spatial pattern formation in interacting turing systems*, Bulletin of mathematical biology, *61*(3) (1999), 483505.

[7] F. Benkhaldoun, A. Halassi, D. Ouazar, M. Seaid, and A. Taik, *A stabilized meshless method for time-dependent convection-dominated flow problems*, Mathematics and Computers in Simulation, *137* (2017), 159176.

[8] M. Dehghan, M. Abbaszadeh, and A. Mohebbi, *The use of element free Galerkin method based on moving Kriging and radial point interpolation techniques for solving some types of Turing models*, Engineering Analysis with Boundary Elements, *62* (2016), 93111.

[9] H. Fatahi, J. SaberiNadjafi, and E. Shivanian, *A new spectral meshless radial point interpolation (smrpi) method for the two-dimensional fredholm integral equations on general domains with error analysis*, Journal of Computational and Applied Mathematics, *294* (2016), 196209.

[10] H. R. Ghehsareh, K. Karimi, and A. Zaghian, *Numerical solutions of a mathematical model of blood flow in the deforming porous channel using radial basis function collocation method*, Journal of the Brazilian Society of Mechanical Sciences and Engineering, *38*(3) (2016), 709720.

[11] A. Gierer and H. Meinhardt, *A theory of biological pattern formation*, Kybernetik, *12*(1) (1972), 3039.

[12] P. Gray and S. K. Scott, *Autocatalytic reactions in the isothermal, continuous stirred tank reactor: isolas and other forms of multistability*, Chemical Engineering Science, *38*(1) (1983), 2943.

[13] P. Gray and S. K. Scott, *Autocatalytic reactions in the isothermal, continuous stirred tank reactor: Oscillations and instabilities in the system* $A+2B \to 3B; B \to C$, Chemical Engineering Science, *39*(6) (1984), 10871097.

[14] V. R. Hosseini, E. Shivanian, and W. Chen, *Local integration of 2-d fractional telegraph equation via local radial point interpolant approximation*, The European Physical Journal Plus, *130*(2) (2015), 33.

[15] W. Hundsdorfer and J. G. Verwer, *Numerical solution of time-dependent advection- diffusion-reaction equations*, Springer Science & Business Media, *33* (2013).

[16] A. Jafarabadi and E. Shivanian, *Numerical simulation of nonlinear coupled burgers' equation through meshless radial point interpolation method*, Engineering Analysis with Boundary Elements, *95* (2018), 187199.

[17] J. P. Kernevez and D. Thomas, *Numerical analysis and control of some biochemical systems*, Applied mathematics and optimization, *1*(3) (1975), 222285.

[18] A. Madzvamuse and A. H. Chung, *Fully implicit time-stepping schemes and non-linear solvers for systems of reactiondiffusion equations*, Applied Mathematics and Computation, *244* (2014), 361374.

[19] A. Madzvamuse and P. K. Maini, *Velocity-induced numerical solutions of reaction-diffusion systems on continuously growing domains*, Journal of computational physics, *225*(1) (2007), 100119.

[20] V. Mošová, *Meshless rkhpu method and its applications*, Mathematics and Computers in Simulation, *76*(1-3) (2007), 161165.

[21] J. D. Murray, *Mathematical biology*, Springer, Heidelberg, New York, 1993.

[22] V. P. Nguyen, T. Rabczuk, S. Bordas, and M. Duflot, *Meshless methods: a review and computer implementation aspects*, Mathematics and computers in simulation, *79*(3) (2008), 763813.

[23] I. Prigogine and R. Lefever, *Symmetry breaking instabilities in dissipative systems, ii*, The Journal of Chemical Physics, *48*(4) (1968), 16951700.

[24] P. Reihani, *A numerical investigation of a reaction-diffusion equation arises from an ecological phenomenon*, Computational Methods for Differential Equations, *6*(1) (2018), 98 110.

[25] K. Saranya, V. Mohan, R. Kizek, C. Fernandez, and L. Rajendran, *Unprecedented homotopy perturbation method for solving nonlinear equations in the enzymatic reaction of glucose in a spherical matrix*, Bioprocess and biosystems engineering, *41*(2) (2018), 281 294.

[26] A. Sayyidmousavi, F. Daneshmand, M. Foroutan, and Z. Fawaz, *A new meshfree method for modeling strain gradient microbeams*, Journal of the Brazilian Society of Mechanical Sciences and Engineering, *40*(8) (2018), 384.

[27] J. Schnakenberg, *Simple chemical reaction systems with limit cycle behaviour*, Journal of theoretical biology, *81*(3) (1979), 389400.

[28] F. Shakeri and M. Dehghan, *The finite volume spectral element method to solve turing models in the biological pattern formation*, Computers & Mathematics with Applications, *62*(12) (2011), 43224336.

[29] A. Shirzadi, V. Sladek, and J. Sladek, *A local integral equation formulation to solve coupled nonlinear reactiondiffusion equations by using moving least square approximation*, Engineering Analysis with Boundary Elements, *37*(1) (2013), 814.

[30] E. Shivanian, *Meshless local petrovgalerkin (* MLPG*) method for three-dimensional nonlinear wave equations via moving least squares approximation*, Engineering Analysis with Boundary Elements, *50* (2015), 249257.

[31] E. Shivanian, *Analysis of meshless local radial point interpolation (* MLRPI*) on a nonlinear partial integro-differential equation arising in population dynamics*, Engineering Analysis with Boundary Elements, *37*(12) (2013), 16931702.

[32] E. Shivanian, *Analysis of meshless local and spectral meshless radial point interpolation (* MLRPI *and* SMRPI*) on 3-d nonlinear wave equations*, Ocean Engineering, *89* (2014), 173188.

[33] E. Shivanian, *A new spectral meshless radial point interpolation (* SMRPI*) method: A well-behaved alternative to the meshless weak forms*, Engineering Analysis with Boundary Elements, *54* (2015) 112.

[34] E. Shivanian, *On the convergence analysis, stability, and implementation of meshless local radial point interpolation on a class of three-dimensional wave equations*, Interna- tional Journal for Numerical Methods in Engineering, *105*(2) (2016), 83110.

[35] E. Shivanian, *Spectral meshless radial point interpolation (smrpi) method to twodimensional fractional telegraph equation*, Mathematical Methods in the Applied Sciences, *39*(7) (2016), 18201835.

[36] E. Shivanian and A. Jafarabadi, *Error and stability analysis of numerical solution for the time fractional nonlinear Schrödinger equation on scattered data of generalshaped domains*, Numerical Methods for Partial Differential Equations, *33*(4) (2017), 1043 1069.

[37] E. Shivanian and A. Jafarabadi, *Inverse cauchy problem of annulus domains in the framework of spectral meshless radial point interpolation*, Engineering with Computers, *33*(3) (2017), 431442.

[38] E. Shivanian and A. Jafarabadi, *Numerical solution of two-dimensional inverse force function in the wave equation with nonlocal boundary conditions*, Inverse Problems in Science and Engineering, *25*(12) (2017), 17431767.

[39] E. Shivanian and A. Jafarabadi, *An inverse problem of identifying the control function in two and three-dimensional parabolic equations through the spectral meshless radial point interpolation*, Applied Mathematics and Computation, *325* (2018), 82101.

[40] E. Shivanian and H. R. Khodabandehlo, *Meshless local radial point interpolation (* MLRPI*) on the telegraph equation with purely integral conditions*, The European Physical Journal Plus, *129*(11) (2014), 241.

[41] V. Sladek, J. Sladek, and A. Shirzadi, *The local integral equation method for pattern formation simulations in reactiondiffusion systems*, Engineering Analysis with Boundary Elements, *50* (2015), 329340.

[42] D. Thomas, *Artificial enzyme membranes, transport, memory, and oscillatory phenomena*, Analysis and control of immobilized enzyme systems, (1975), 115150.

[43] A. M. Turing, *The chemical basis of morphogenesis*, Philosophical Transactions of the Royal Society of London, Series B, Biological Sciences, *237*(641) (1952), 3772.

[44] E.H. Twizell, A.B. Gumel, and Q. Cao, *A second-order scheme for the Brusselator reactiondiffusion system*, Journal of Mathematical Chemistry, *26*(4) (1999), 297316.

[45] J. Zhu, Y. T. Zhang, S. A. Newman, and M. Alber, *Application of discontinuous Galerkin methods for reaction-diffusion systems in developmental biology*, Journal of Scientific Computing, *40*(1-3) (2009), 391418.